RADIATIVE FORCING OF SAHARAN DUST: GOCART MODEL SIMULATIONS COMPARED WITH ERBE DATA

Clark J. Weaver
GEST Institute, Rockville, Maryland
weaver@demeter.gsfc.nasa.gov

Paul Ginoux
Georgia Tech
N. Christina Hsu
GEST/UMBC
Ming-Dah Chou and Joanna Joiner
NASA Goddard Space Flight Center, Greenbelt, Maryland 20771 USA

August 23, 2001

Abstract

This study uses information on Saharan aerosol from a dust transport model to calculate radiative forcing values. The transport model is driven by assimilated meteorological fields from the Goddard Earth Observing System Data Assimilation System. The model produces global three-dimensional dust spatial information for 4 different mineral aerosol sizes. These dust fields are input to an off-line radiative transfer calculation to obtain the direct radiative forcing due to the dust fields. Our estimates of the short wave reduction of radiation at the top of atmosphere (TOA) compare reasonably well with the TOA reductions derived from ERBE and TOMS satellite data. The long wave radiation also agrees with the observations; however potential errors in the assimilated temperatures complicate the comparison. Depending on the assumptions used in the calculation and the dust loading, the summertime forcing ranges from 0 to -18 Wm^{-2} over ocean and 0 to +20 Wm^{-2} over land.

Increments are terms in the assimilation general circulation model (GCM) equations that force the model toward observations. They are differences between the observed analyses and the GCM forecasts. Off West Africa the analysis temperature increments produced by the assimilation system show patterns that are consistent with the dust spatial distribution. We do not believe that radiative heating of dust is influencing the increments. Instead, we suspect that dust is affecting the TOVS satellite temperature retrievals which provide the basis of the assimilated temperatures used by the model.

1 Introduction

On a local scale mineral aerosol (dust) can significantly impact the atmospheric radiation budget (Carlson and Benjamin, 1980; d'Almeida, 1987; and Li et al., 1996) but determining the magnitude of forcing on a global scale is uncertain. This is due to limited information on the global spatial distribution of dust and uncertainties in the optical parameters of the dust.

Currently, the only approach to obtaining the dust size and spatial distributions on a global scale is simulation by a General Circulation Model (GCM). A recent series of papers (Tegen et al. 1996; Miller and Tegen, 1998) use the Goddard Institute for Space Studies (GISS) GCM to simulate the dust distributions and in turn the global radiative forcing, but there are issues with the dust source location and its strength in the GISS GCM. Our study uses a transport model driven by assimilated winds and a new formulation of the dust source described in Ginoux et al (2001) to obtain three-dimensional dust spatial information for various size ranges. In contrast to GCM winds, assimilated winds allow comparison of model-derived aerosol concentrations with actual observations during a specific event. The simulated dust fields compare well with the spatial dust patterns in the Aerosol Index (AI, see Herman et al, 1997) derived from the Total Ozone Mapping Spectrometer (TOMS) and ground-based dust concentrations. The significance of our study is that dust spatial distributions used in the radiative calculations are validated to some degree by observations.

Besides the spatial distribution, information on the dust optical parameters (OP) are necessary for any radiative calculations. Until recently, most OP information, used in published radiative forcing studies, was derived from Mie scattering theory from samples of Saharan dust (Patterson, 1977). Because of the paucity of dust OP for different source regions, these parameters are used on the global scale. Although more information on OP is emerging for other regions, one can only make an educated guess on the range of OP on the global scale.

Most of the recent calculations on aerosol forcing, Tegen et al (1996), Carlson and Benjamin (1980) consider only the direct effect of the aerosols on the radiative fluxes and do not account for any feedbacks between aerosols and the atmospheric fields. Miller and Tegen (1998) are able to address some of these feedbacks using the GISS-GCM. Presence of aerosols can also indirectly change the radiative fluxes by altering the cloud condensation nuclei concentrations and finally the cloud albedo (Twomey, 1977). Our results only account for the direct change in the radiative fluxes due to the presence of aerosols and cannot account for cloud induced indirect effects. We should not necessarily expect close similarity with forcing rates derived from observations which will include both the direct and indirect effects.

2 GOCART Dust model

The dust model is fully described in Ginoux et al 2001. It is an off-line transport model driven by assimilated meteorological fields from the Goddard Earth Observing System Data Assimilation System, GEOS-1 (Schubert et al., 1993). The GOCART runs on the same vertical and horizontal grid used in GEOS-1: $2.0°$ latitude by $2.5°$ longitude and 20 vertical levels with 5 in the boundary layer. The model transports four size ranges from .1 to 10 micron using a three-dimensional flux form semi-Lagrangian scheme (Lin and Rood, 1996). The dust source module is based on archived surface wetness, local wind speed and eddy diffusion. The module requires an estimate of the total global emission. A value of 2000 teragram / year seems to yield concentrations that are in good agreement with the groundbased observations. The GOCART model accounts for convective and diffusive transport by using archived cloud convective mass flux and vertical eddy diffusion coefficients. Removal by wet deposition requires three-dimensional precipitation information which is estimated from the assimilation two-dimensional precipitation fields. The model accounts for gravitational settling.

The radiative calculations were done using temperature, moisture, cloud and albedo fields from the GEOS-2 assimilation. The vertical grid used has about twice the resolution of the GEOS-1 grid. The dust fields were vertically interpolated onto the lowest layers preserving the total column loading on the GEOS-1 grid. The radiative transfer code (Chou and Suarez, 1999 and Chou and Suarez, 1994) is modified from the GEOS-2 GCM to account for the spatial variability and spectral dependence of aerosols. The GEOS-2 radiation model and meteorological fields provided more accurate information of the effect of clouds, but results of cloudy conditions are not presented here.

Presence of aerosols will modify the bulk scattering properties of a layer according to the aerosol optical depth (τ), single scattering albedo (ω) and asymmetry factor (g) at a given wavelength (λ).

These three dimensional fields are weighted by the mass of dust in each grid box m for each particle of the four particle sizes (i) as simulated by the transport model. The optical parameters, extinction coefficient $(Q_{ext}), \omega_0$ and g_0 are based on Mie scattering theory from Saharan dust samples. At any location in latitude and longitude (x, y) we calculate the (τ), (ω), (g) at each vertical grid level z where rad_{ef} is the effective radius and ρ is the particle mass density.

$$\tau_i(z, \lambda) = (3/4) * m(z, i) * Q_{ext}(i, \lambda)/(rad_{ef}(i) * \rho(i)) \tag{1}$$

$$\tau(z, \lambda) = \sum_{i=1}^{i=4} \tau_i(z, \lambda) \tag{2}$$

$$\omega(z, \lambda) = \frac{\sum_{i=1}^{i=4} \tau_i(z, \lambda) * \omega_0(i, \lambda)}{\tau(z, \lambda)} \tag{3}$$

$$g(z, \lambda) = \frac{\sum_{i=1}^{i=4} \tau_i(z, \lambda) * \omega_0(i, \lambda) * g_0(i, \lambda)}{\omega(z, \lambda) * \tau(z, \lambda)} \tag{4}$$

Values of Q_{ext}, ω_0 and g_0 are highly uncertain since they depend on mineral composition of the dust source which varies globally (Sokolik and Toon, 1999). These optical parameters are calculated from Mie theory using indices of refraction derived from laboratory analysis or satellite measurements.

Sokolik and Toon, (1996) present optical parameters in the solar band from several previously published dust models. For a given wavelength and particle size, the models have very different levels of single scattering albedo (ω_0). At $\lambda = 550\mu$m and particle radius 1.5μm, the World Meteorological Orgainization reports ω_0 of 0.64, Tegen and Lacis (1996) report 0.86, and Kaufman et al (2001) report 0.97. The Kaufman parameters are derived from groundbased sunphotometers and Landsat measurements over Senegal during spring of 1987. Since there is no accepted set of dust optical parameters to use for radiative forcing calculations, we present results that span the accepted range of absorption.

We present one set of radiative forcing calculations that use optical parameters (OP) from Patterson, (1977) which are moderately absorbing. Patterson (1977) analyzed dust samples from different locations in the Sahara and Barbados. They report real and imaginary refractive indices in the solar and infrared that are almost invariant with the sampling location. The actual values we use for our calculations are reported by Tegen and Lacis (1996) and have slightly higher absorption than those from Patterson's original values.

A second set of forcing calculations assume the particles are composed of pure illite. This is a type of clay which is almost non-absorbing in the visible. Refractive indices are reported in the solar frequencies (Egan and Hilgeman, 1979) and in the infrared (Query, 1987). Figure 1 compare the single scattering albedos for 1 micron particles in both the short and long wave spectrum.

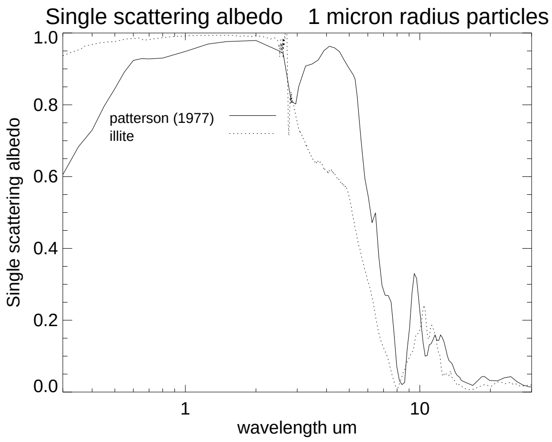

Figure 1: Mie scattering calculations of single scattering albedo of 1 micron particles assuming indices of refraction 1) from Patterson (1977) as modified by Tegen and Lacis (1996) (solid line) and 2) for pure illite, Egan and Hilgeman (1979) and Query (1987) (dotted line)

The solar radiative transfer routine accounts for absorption by water vapor, ozone, CO_2, O_2, clouds, and aerosols and accounts for scattering by clouds, aerosols, and gases. The solar spectrum (.2 to 10 um) is divided into eight bands in the UV to visible range and three IR bands. The infrared radiative transfer calculation accounts for water vapor, CO_2, O_3, trace gases, clouds, and aerosols. The IR spectrum (3 to 100 μ) is divided into ten bands. In addition to the aerosol information, the radiative transfer code requires fields of temperature, specific humidity, cloud optical thickness, cloud fraction and albedoes. The GEOS-2 assimilation archives all the fields required for the transport model and the radiative calculations.

For each day of interest the solar and infrared radiative fluxes were calculated using meteorological variables archived from the assimilation. First we calculate the radiative fluxes for a clean (dust free) atmosphere using only the meteorological variables, $\mathbf{F}_{clean}$. Then we calculate the radiative flux for a dusty atmosphere, $\mathbf{F}_{dust}$ using the τ, ω, and g derived from output from the dust transport model. The difference in the radiative fluxes, $\mathbf{F}_{dust}$ - $\mathbf{F}_{clean}$ = $\Delta\mathbf{F}$ is only due to the 'direct' influences from the dust. Since both calculations use the same archived meteorological fields, indirect feedbacks are not included.

3 Top of atmosphere Radiative Fluxes

3.1 Comparison with ERBE Fluxes

We compare our Top of atmosphere (TOA) results with observations derived from Earth Radiation Budget Satellite (ERBE) and the TOMS AI. The ERBE measured SW and LW broadband irradiance from the earth-atmosphere system. Since the motivation of this study is climate forcing, our convention throughout this paper is that downward fluxes are positive. The outgoing LW and backscattered SW radiation impinging on ERBE will be negative. Hsu et al (2000) (hereafter referred to as HHW) has extracted the sensitivity in the ERBE irradiances to the dust atmospheric loading as determined from the TOMS AI over part of the Sahara (29 - 33 N: 5W - 15E) using data from July 1985. The approach was to bin both the TOMS AI and ERBE fluxes onto 1° latitude by 1° longitude grids. Data from the HIRS instrument (which flew on the same satellite as ERBE) was used to remove points contaminated by clouds and high water vapor. The remaining clear sky data points were sorted by the underlying surface (land vs. ocean) and linearly regressed. The slope, $\partial\mathbf{F}_{ERBE}\downarrow/\partial\mathrm{AI}$ is the sensitivity factor (the $\downarrow$ means that downward radiation is positive). Over ocean for both bands and over land in the LW band, HHW found a linear relationship between atmospheric loading and TOA radiative fluxes. However, over land there was no relationship between loading and SW TOA fluxes. Since HHW only considered clear sky conditions, the GOCART radiative fluxes used for comparison are for clear sky only. Figure 2a shows the SW and Figure 2b the LW August dust radiative forcing at 1430 local time generated by multiplying $\partial\mathbf{F}_{ERBE}\downarrow/\partial\mathrm{AI}$ derived from July 1985 by the monthly mean August 1988 TOMS AI. At any location the ERBE satellite passes overhead at 1430 local time and samples the data used to derive $\partial\mathbf{F}_{ERBE}\downarrow/\partial\mathrm{AI}$.

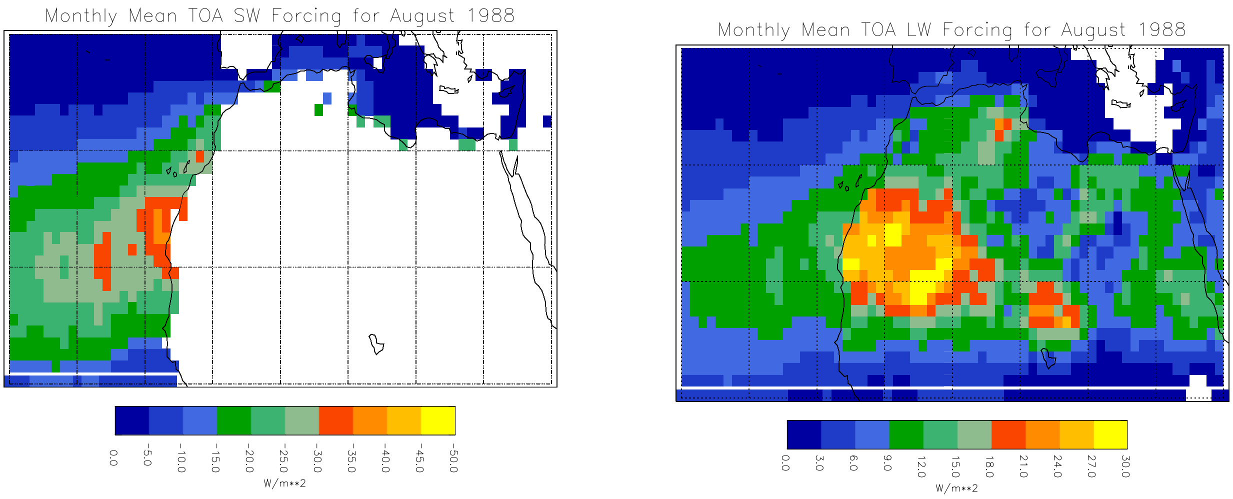

Figure 2: Monthly Mean TOA short and long wave forcing for August 1988 derived from ERBE radiative fluxes and TOMS Aerosol Index observations. Downward fluxes are positive. Presence of dust increases the outgoing SW radiation, reduces the net downward SW radiation, hence forcing values are negative. Dust reduces the outgoing LW, increases the net downward LW, hence forcing are positive. All values are at 1430 local time.

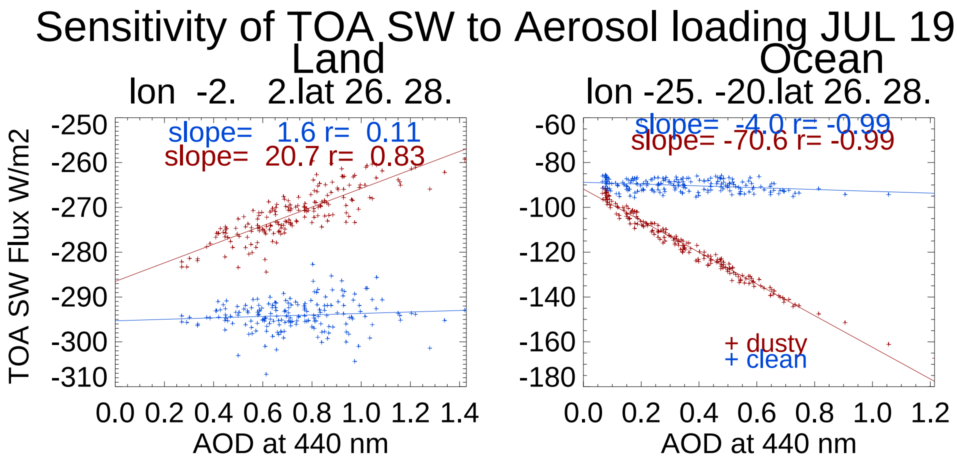

Figure 3: Regression of outgoing TOA SW flux calculations against AOD in GOCART model during July 1988. On any given day each grid point will have a vertical profile of dust from the GOCART model, a short wave flux, $\mathbf{F}_{dust}$ calculated using this profile and a flux that assumes a clean atmosphere $\mathbf{F}_{clean}$. Both fluxes are plotted against the AOD from the GOCART profile using a red point for $\mathbf{F}_{dust}$ and a blue point for $\mathbf{F}_{clean}$. Shown are regressions within a single 2° latitude by 5° longitude geographic box over land (left panel) and a single geographic box over ocean (right panel). Large pluses are one pair of points for a single time-location, see text. Patterson OP are used. Our sign convention has outgoing fluxes as negative.

3.1.1 Shortwave comparison

Comparing the observed and modeled sensitivity of TOA flux to aerosol optical depth (AOD) is a simple test of the optical parameters. HHW convert the aerosol index to AOD at 440 nm using the linear relationships found at various sites in the Sahara (Hsu et al, 1999). They estimate that in summer over ocean the change in TOA SW $\mathbf{F}\downarrow$ per unit AOD at 440 nm ($\partial\mathbf{F}\downarrow/\partial\mathrm{AOD}_{440}$) at 1430 local time is 60 Wm^{-2} . We calculate the SW forcing sensitivity of the GOCART model by first time-interpolating the assimilated meteorological fields to 1430 local time. Then we perform radiative calculations that assume a dust distribution from the GOCART model, $\mathbf{F}_{dust}$ and radiative calculations that assume no dust $\mathbf{F}_{clean}$. Figure 3 shows the scatter of SW TOA $\mathbf{F}\downarrow$ from both calculations plotted against the AOD from the GOCART model assuming Patterson (OP). The red points are for calculations that include the GOCART dust and the blue points assume a clean atmosphere. As expected, the blue points show no relationship with the AOD in the GOCART model.

We calculated our SW TOA $\partial\mathbf{F}\downarrow/\partial\mathrm{AOD}_{440}$ using the same latitude domain used in HHW and compare results in Table 1. Over ocean our calculated $\partial\mathbf{F}\downarrow/\partial\mathrm{AOD}_{440}$ of -66 Wm^{-2} using Patterson OP is close to the TOMS/ERBE estimate of -60 Wm^{-2} . Over ocean the model-observation comparison is robust because the ocean surface albedo used in the GEOS-2 assimilation is accurate. Over land the surface albedo is less certain and may complicate the comparison. Both Patterson and illite OP show some sensitivity with AOD but the TOMS/ERBE analysis show none.

Table 1: Sensitivity of TOA $\mathbf{F}_{dust}$ in Wm^{-2} per AOD at 440 nm ($\partial\mathbf{F}\downarrow/\partial\mathrm{AOD}_{440}$) during July

	Month	SW		LW	
		land	ocean	land	ocean
Patterson	July 1988	+22	-66	+37	+19
Illite	July 1988	-28	-81	+41	+21
HHW	July 1985	-[a]	-60	+36	+24

[a] HHW analysis showed no correlation between ERBE flux and AOD

The monthly mean SW TOA $\Delta\mathbf{F}\downarrow = \mathbf{F}_{dust}\downarrow - \mathbf{F}_{clean}\downarrow$ at 1430 local time is shown in Figure 4. The values over land have been masked for comparison with (Figure 2a). Use of the Patterson OP yields good agreement with the observed TOA forcing (Figure 2a); the model forcing is -35 to -40 Wm^{-2} near the African coast and -30 to -35 Wm^{-2} in the open ocean. The TOMS/ERBE estimates show about 5 Wm^{-2} less forcing. The model forcing using illite OP is slightly higher than the Patterson OP forcing.

3.1.2 Longwave comparison

Comparisons of modeled and observed longwave radiation are complicated by the sensitivity of longwave radiation to the water vapor content and the temperature. One dimensional radiative tests, detailed in HHW (Hsu et al, 2000), show that the radiative impact of dust is reduced in the presence of moisture. To remove the effect of water vapor, only conditions of lower precipitable water ($<$3cm) were used in the HHW analysis. Over land the ERBE measurements shows a linear increase in the longwave TOA radiation with aerosol loading. The HHW analysis estimate that in summer the TOA LW $\partial\mathbf{F}\downarrow/\partial\mathrm{AOD}_{440}$ is 36 Wm^{-2} .

The GEOS-2 assimilation provides fields of moisture that are used in our radiative calculations. This allows us to analyze radiation calculations with similar column water amounts. Of course, temperature of the surface and atmosphere also influence the longwave ERBE fluxes. HHW do their calculations of longwave sensitivity over small ($4°$ latitude by $5°$ longitude) areas of land. On days when there is no dust present, any variability in the longwave fluxes is largely due to fluctuations in temperature (e.g from a passing synoptic event). On days when dust is present the increase in the TOA ERBE longwave fluxes is due to the green house effect as well as any influence the dust may have on temperature. Our analysis bins the model radiation calculations by column moisture at a 1 cm resolution and surface temperature at a 3 (K) resolution. Figure 5 shows the scatter of TOA LW $\mathbf{F}\downarrow$ from the model for dust (red) and clean (blue) calculations plotted against the AOD from the GOCART model. It is similar to Figure 3 except that instead of binning for location, the binning is for surface temperature and moisture content. Shown are all land points with a surface temperature close to 324 K. The two panels are for a water column bins centered at 1.5 and 2.5 cm. Over land HIRS2 measurements of precipitable water and sunphotometer observations usually are between 1-6 cm so the regressions shown are for relatively dry conditions. Slopes from regression plots for other surface temperatures and moisture contents are shown in Table 2. The general trend is that $\partial\mathbf{F}\downarrow/\partial\mathrm{AOD}_{440}$ is reduced as moisture content increases and surface temperature decreases.

We calculate the $\partial\mathbf{F}\downarrow/\partial\mathrm{AOD}_{440}$ only using model data that matched the same conditions used in HHW TOMS/ERBE estimates. Our calculations only include points for the driest conditions (precipitable water $<$3cm). Table 1 shows our calculated and the HHW observed flux sensitivity

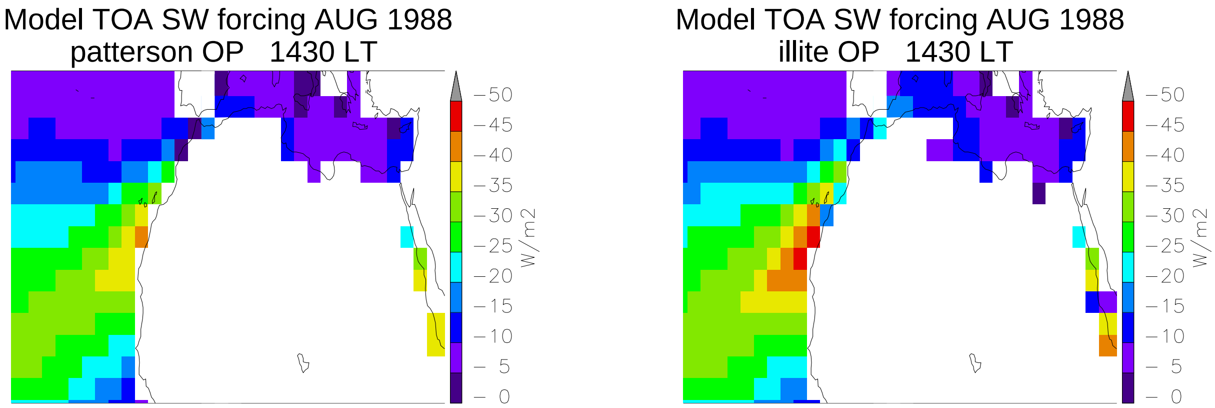

Figure 4: Monthly Mean TOA short wave $\Delta\mathbf{F}\downarrow = \mathbf{F}_{dust}\downarrow - \mathbf{F}_{clean}\downarrow$ for August 1988 using OP from (a) Patterson (1977) and (b) illite. All values are at 1430 local time.

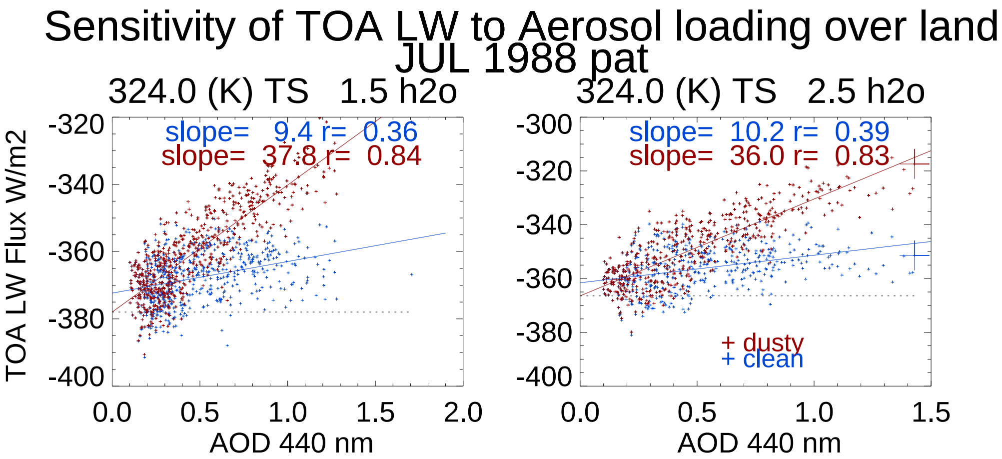

Figure 5: Regression of outgoing TOA LW flux calculations against AOD in GOCART model during July 1988. On any given day each grid point will have a vertical profile of dust from the GOCART model, a long wave flux $\mathbf{F}_{dust}$ calculated using this profile and a flux that assumes a clean atmosphere $\mathbf{F}_{clean}$. Both fluxes are plotted against the AOD from the GOCART profile using a red point for $\mathbf{F}_{dust}$ and a blue point for $\mathbf{F}_{clean}$. Shown are regressions for grid locations over land with a surface temperature between 322.5-325.5 (K) during July 1988. The left panel has points with column water between 1.0-2.0 cm (very dry), the right panel has points between 2.0-3.0 cm (dry). Radiative calculations assume Patterson OP. Our radiation sign convention has outgoing fluxes as negative.

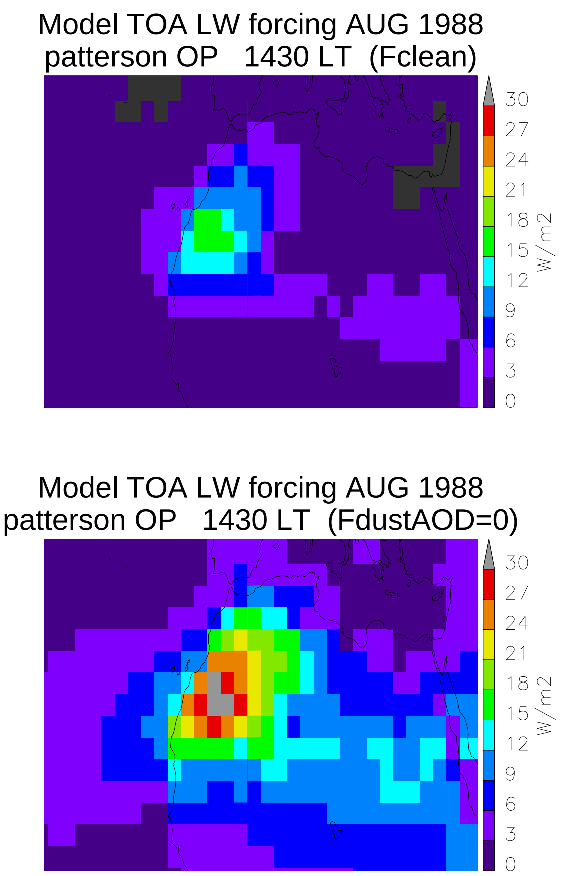

Figure 6: Monthly Mean TOA long wave $\Delta\mathbf{F}\downarrow = \mathbf{F}_{dust}\downarrow - \mathbf{F}_{clean}\downarrow$ for August 1988 using optical parameters from (a) Patterson (1977) and (b) illite. Monthly Mean TOA long wave $\Delta\mathbf{F}\downarrow = \mathbf{F}_{dust}\downarrow - \mathbf{F}_{dust}\downarrow$ (AOD=0) for August 1988 using optical parameters from (c) Patterson (1977) and (d) illite. All values are at 1430 local time.

per change in AOD 440 for July. Both Patterson and illite OP yield a model sensitivity that closely matches the HHW observations. However, both our two estimates for the monthly mean forcing (Figure 6ab) are significantly less than the observed value (Figure 2b). The difference between HHW and our forcing calculations lie in the flux values used for clean conditions. In Figure 6ab the flux values used for clean conditions are the $\mathbf{F}_{clean}\downarrow$ values and are plotted as the blue points in Figure 5. However, in HHW the flux values used for clean conditions are the flux value where AOD=0 on the dust (red) points regression line, $\mathbf{F}_{dust}\downarrow$ (AOD=0). This is shown by the flat dotted black line.

An alternative longwave forcing calculation that uses the $\mathbf{F}_{dust}\downarrow$ (AOD=0) as the flux value for clean conditions is shown in Figure 6cd. To illustrate the difference between the two methods of $\Delta\mathbf{F}\downarrow$ calculation, consider a high AOD condition and column moisture of 2.5 cm (large plus points on second panel of Figure 5). When $\Delta\mathbf{F}\downarrow = \mathbf{F}_{dust}\downarrow - \mathbf{F}_{clean}\downarrow$, the forcing is +34 Wm^{-2} (-318 minus -352), but when $\Delta\mathbf{F}\downarrow = \mathbf{F}_{dust}\downarrow - \mathbf{F}_{dust}\downarrow$ (AOD=0) the forcing is +49 Wm^{-2} (-318 Wm^{-2} minus the regression line intercept at AOD=0 of -367 Wm^{-2}). The monthly mean LW radiative forcing calculation where $\Delta\mathbf{F}\downarrow = \mathbf{F}_{dust}\downarrow - \mathbf{F}_{dust}\downarrow$ (AOD=0) involves binning the daily flux values for each GOCART grid point. Over ocean we tried to reproduce the HHW analysis by binning over small boxes (5° longitude and 3° latitude). Over land we binned by surface temperature and moisture content. The points within each bin were linearly regressed (figure Figure 5 shows results of several bins). Those bins that had narrow ranges of AOD did not exhibit a good correlation between TOA flux and AOD, and were not considered. The slopes for July 1988, assuming Patterson OP, are shown in Table 2. Every grid point has an associated daily value of moisture column, surface temperature and AOD. To calculate the $\Delta\mathbf{F}\downarrow = \mathbf{F}_{dust}\downarrow - \mathbf{F}_{dust}\downarrow$ (AOD=0) we simply multiply the applicable slope by the AOD.

An interesting aspect of Figure 5 is the negative correlation $\mathbf{F}_{clean}$ (blue points) has with AOD from the GOCART model. The radiative calculations for these points only use the GEOS-1 temperature, water vapor profiles; no aerosol information from GOCART was part of these calculations. This unexpected correlation arises because dust in the real atmosphere is somehow influencing the assimilated temperatures.

Table 2: Sensitivity of TOA LW $\mathbf{F}_{dust}$ per AOD 440 ($\partial\mathbf{F}\downarrow/\partial\mathrm{AOD}_{440}$)for July 1988 over land

Temperature	Column	Moisture	cm
Surface (K)	1.5	2.5	3.5
314	27	20	-[a]
316	31	21	15
318	37	25	19
320	36	27	19
322	34	33	23
324	38	36	23
326	45	36	27
328	47	37	35

[a] There were not enough points for a good regression

3.2 Daily forcing estimates

All radiative forcing calculations presented so far have been at 1430 LT. We now change our focus to climate forcing and consider mean daily estimates. As before, positive values of $\Delta\mathbf{F}\downarrow$ describe increased incoming or decreased outgoing radiation. Positive values of $\Delta\mathbf{F}\downarrow$ at the top of the atmosphere from aerosol indicates warming of the entire earth-atmosphere system by aerosols. Figure 7ab shows the shortwave TOA $\Delta\mathbf{F}\downarrow$ for June,July and August (JJA) 1988 using both Patterson and illite OP. Radiative calculations were done at 9, 12 and 15 hours local time and weighted to yield a daily value. The $\Delta\mathbf{F}\downarrow$ SW TOA is largely explained by two factors: Absorption of solar radiation by dust and differences between the albedo of the dust and the underlying surface.

Over oceans the dust increases the outgoing shortwave radiation since it is a much better reflector than the underlying dark water. This difference in reflectivity dominates the solar absorption by the dust. Presence of dust increases reflected solar radiation and decreases the net downward solar flux at the TOA. Dust composed of illite is more reflective than dust assuming Patterson OP so the radiative forcing is more negative for the illite calculations.

Over land dust that assumes the Patterson OP is more absorbing than the underlying reflective desert. The dust absorbs and scatters the incoming solar radiation and also absorbs and reduces the reflected solar radiation. Both contribute to reduce the outgoing solar radiation and increase the net downward flux at TOA. When illite is assumed, the dust is more reflective than the desert and decreases the net downward solar flux at the TOA.

The LW forcing is calculated for $\Delta\mathbf{F}\downarrow$ = $\mathbf{F}_{dust}\downarrow$ - $\mathbf{F}_{clean}\downarrow$ (not shown) and $\Delta\mathbf{F}\downarrow$ = $\mathbf{F}_{dust}\downarrow$ - $\mathbf{F}_{dust}\downarrow$ (AOD=0) (Figure 7cd) . Both calculations were done at 0, 6, 12 and 18 hours local time and averaged to yield a daily value. In the longwave band the dust absorbs terrestrial radiation and generally reemits it at lower temperature than the underlying surface. Presence of dust reduces the outgoing longwave radiation and increases the downward TOA longwave flux. Figure 7 shows the strongest forcing over West Africa where the model has the highest dust atmospheric loading. Over ocean the difference between the dust and the underlying surface temperature is less pronounced than over land. This effect reduces the dust TOA perturbation over ocean.

Estimates of the JJA net TOA flux perturbation are shown in Figure 8. Depending on the assumptions used in the calculation and the dust loading, the forcing ranges from 0 to -18 Wm^{-2} over ocean and 0 to 20 Wm^{-2} over land.

4 Surface Radiative Fluxes

Positive values of $\Delta\mathbf{F}\downarrow$ at the earth's surface indicate that the dust is warming the Earth. The dominate contribution is the reduction of SW at the earth's surface due to dust scattering and absorption. Less of a factor is the increase in the downward LW radiation, since the dust layer radiates at a much warmer temperature than the clear sky. Figure 9 shows the net (SW+LW) $\Delta\mathbf{F}\downarrow$ at the Earth's ground surface for August 1988.

5 Heating Rates

The $\Delta\mathbf{F}\downarrow$ at TOA indicates forcing of the earth-atmosphere system; $\Delta\mathbf{F}\downarrow$ at the earths surface indicates forcing of only the earth. The TOA forcing minus the forcing at the earths surface indicates the forcing on the atmosphere only. Consider the Patterson OP case assuming that $\Delta\mathbf{F}\downarrow$ = $\mathbf{F}_{dust}\downarrow$ - $\mathbf{F}_{dust}\downarrow$ (AOD=0) . The TOA values over West Africa are above 12 Wm^{-2} (Figure 8a) but at the surface there is cooling of 20 to 25 Wm^{-2} (Figure 9a). This difference indicates a strong warming of the atmosphere system. The dust vertically redistributes the thermal structure of atmosphere since it cools the surface and warms the air above.

Our radiative transfer model using the GOCART dust fields also calculates heating rates. The heating rate perturbation due to dust is simply the heating rate assuming the GOCART dust profiles minus the rate assuming clean conditions. We calculate maximum monthly mean August values of 2 degrees per day over the Sahara. This is consistent with the estimates from Carlson and Benjamin (1980) of several degrees per day net heating for a cloud free desert case during heavy loading conditions (optical thickness of 1).

The analysis temperature increments produced by the assimilation system may provide information on the indirect radiative impact of the dust. Increments are terms in the assimilation general circulation model (GCM) equations that force the model toward observations. They are differences between the observed analyses and the GCM forecasts. The National Environmental Satellite Data and Information Service (NESDIS) provide temperature retrievals from the TIROS Operational Vertical Sounder (TOVS) radiances. These NESDIS-TOVS temperatures dominate the observed analyses over ocean. Positive (Negative) increments indicate that the GCM is too cold (warm). The increments are the sum of all model and intial condition errors in the GCM. A correlation between our calculated radiative forcing fields and the temperature increments indicates that the increments are compensating for the lack of aerosol transport and radiative effects in the assimilation. Figure 10ab shows the assimilation increments derived from the TOVS temperature retrievals (upper panels) and the estimated heating rates from the Patterson parameters at 00Z (lower panels). At 00Z when there is no solar heating off the African coast, the model shows weak LW heating at the lowest layer and weak LW cooling above. The increments show a pattern and sign similar to the heating rates, however they are of much larger magnitude. At 12Z (Figure 10cd) the model heating rates responds to the solar heating with strong positive heating rates (1 degree/day). If the TOVS increments were influenced by aerosol heating they would also respond by becoming positive at 12Z to reflect the solar heating. However, at the lower layer the onset of daylight actually reduces the TOVS increments (Figure 10cd) and at the higher layer the increments become more negative. Still, over the Atlantic the increments show a pattern that resembles the tongue of dust transported off Africa. Alpert et al (1998) also report a similarity in the monthly mean fields of assimilation increments and dust over the eastern tropical North Atlantic. This indicates that there is another mechanism associated with the dust besides the radiative heating of dust that is influencing the increments.

We now investigate the potential impact of dust on the TOVS retrievals. This effect, instead of the heating rates, may control the increment patterns over the Sahara region. We use the radiative transfer model of Susskind et al (1983) to simulate TOVS radiances at 21 channels assuming a cloud free atmosphere. Seventeen channels were in the infrared spectrum 667-2514 $cm^{-}1$ (4-15 microns) and 4 in the microwave 50.3-58 Ghz. Meteorological fields are from GEOS-DAS and dust concentration are from the GOCART model. We retrieve two sets of temperature and moisture profiles from these simulated radiances using the DAO TOVS retrieval system of Joiner and Rokke (2000). One set assumes a clean atmosphere T_{clean}, the other a dusty atmosphere, T_{dust}. Figure 11b-d shows the difference in the retrieved temperatures. The correct retrieval, T_{dust} is often more than a degree warmer than the retrieval that does not account for the dust, T_{clean}. Larger effects may be possible, but are discarded by the Quality Contol Scheme. Grey denotes regions where there are no TOVS observations or where the retrievals have been discarded. This can occur either because the residuals between the observed radiances and those computed at convergence are too large or the retrieval scheme does not converge.

Retrievals from actual observed radiances are under investigation. Preliminary results show that in the best circumstances the presence of dust will cause the retrieval algorithm to return a bad quality control flag. Although no contamination will occur, it will preclude retrievals over areas with significant aerosol loading. The operational NESDIS temperature retrievals are available even in locations with heavy aerosol loading, suggesting that these retrievals may be contaminated by aerosols.

6 Discussion

There is often a correlation between LW TOA $\mathbf{F}_{clean}$ (blue points in Figure 5) and the AOD in the GOCART model. This correlation is realized when moisture content and surface temperature are restricted to a narrow range by binning. Since the GOCART model is driven by assimilated winds, it will accurately simulate increased AOD during a real dust event. Somehow information about a real event is also influencing the GEOS-2 assimilation temperatures.

One explanation is that the dust shades the atmosphere below and cools the surface and atmospheric column. This is consistent with reduced outgoing (less negative) $\mathbf{F}_{clean}$ values and increasing AOD. Another mechanism involves a systematic negative bias in the assimilation temperatures compared with the actual temperature on the order of a degree. Recall that the assimilation draws to the

NESDIS-TOVS temperature retrievals which may be contaminated by the dust. Presence of dust can reduce the NESDIS-TOVS temperature retrievals, which will reduce the assimilation temperatures, which will reduce the out going longwave radiation *even if no dust loading is assumed in the radiation calculation*. In general the slopes of the blue points in plots like Figure 5 are about +10 Wm^{-2} per AOD. If we assume that one AOD will cause a one degree error in the assimilated temperatures, the reduction in the longwave broadband radiation is 7 $\mathrm{Wm}^{-2}\dot{(}d\mathrm{LW} = 4{*}\sigma{*}\mathrm{T}^3 * d\mathrm{T}$, where σ is Stefan-Boltzmann constant and T=324 K) This would also explain the reduction in the long wave radiation with increasing AOD in the GOCART model even when no dust loading is assumed in the radiation calculation.

The effect of dust on the TOVS retrievals is a potentially serious complication in the assessment of aerosol climate effects. If the error of the NESDES-TOVS retrievals from dust effects is significant there is no reason to assume that the ERBE measurements are immune either. The bidirectional models that convert the ERBE radiances to TOA fluxes account for aerosols only in a mean sense. Information about dust spatial variability is not included in the bidirectional models.

7 Conclusion

Using a three-dimensional aerosol model and a radiative transfer package we calculate the broadband SW and LW estimates of the radiative forcing perturbation due to Saharan aerosol. We attempt to validate these radiative forcing calculations by comparison with observed forcing estimates using combined TOMS and ERBE data (Hsu et al., 2000). Both optical parameters (OP) considered in this study yield $\partial \mathbf{F}{\downarrow}/\partial \mathrm{AOD}_{440}$ that are within the uncertainties of the observations for the SW and LW bands. However, Patterson OP comes closest to reproducing the TOMS/ERBE estimate in the SW over ocean. In the LW over ocean the Patterson and illite OP behave similarly.

Our radiative forcing calculations suggest that the assimilated atmospheric temperatures are affected by the dust. The temperatures in the assimilation are drawn to temperature retrievals from the TOVS radiances. We show that dust can potentially underestimate the temperature retrievals from the TOVS radiances on the order of a degree K.

The effect of the dust on the assimilated atmospheric temperatures complicates our LW TOA summertime forcing estimates. When we include this effect, our LW calculations agree nicely with the

TOMS/ERBE observations. Calculations without the effect are significantly less than the observations. Depending on the assumptions used in the calculation and the dust loading, the summertime forcing ranges from 0 to -18 Wm^{-2} over ocean and 0 to +20 Wm^{-2} over land (Figure 8) .

Acknowledgments. We thank Arlindo da Silva, Ina Tegen, Andrew Lacis, Yoram Kaufman and two anonymous reviewers.

8 References

d'Almeida, G. A, 1987. On the variability of desert aerosol radiative characteristics., J. Geophys. Res., 92, 3017-3026.

Alpert, P., Y. J. Kaufman, Y. Shay-el, D. Tanre, A. da Silva, S. Schubert, and Y. H. Joseph, 1998: Dust forcing of climate inferred from correlations between dust data and model errors, Nature, 395, 367-370.

Carlson, T. N. and S. G. Benjamin, 1980: Radiative heating rates for Saharan Dust, J. Atmos. Sci., 37, 193-213.

Charlson, R. J., S. E. Schwartz, J. M. Hales, R. D. Cess, J. A. Coakley, Jr., J. E. Hansen, and D. J. Hofmann, 1992:Climate forcing by anthropogenic aerosols, Science, 255, 423-430.

Chou, M., M. J. Suarez, 1994: Technical Report Series on Global Modeling and Data Assimilation: Volume 3 An Efficient Thermal Infrared Radiation Parameterization for use in General Circulation Models, edited by M. J. Suarez, NASA Technical Memorandum 104606.

Chou, M., M. J. Suarez, 1999: Technical Report Series on Global Modeling and Data Assimilation: Volume 15 A Solar Radiation Parameterization for Atmospheric Studies, edited by M. J. Suarez, NASA Technical Memorandum 104606.

Ginoux, P., M. Chin, I. Tegen, J. Prospero, B. Holben, O. Dubovik, and S.J. Lin, 2001: Sources and distributions of dust aerosols simulated with the GOCART model. *J. Geophys. Res.*. in press

Herman, J. R., P. K. Bhartia, O. Torres, C. Hsu, C. Sftor and E. Celarier, 1997: Global distribution of UV-absorbing aerosols from Nimbus 7/TOMS data, J. Geophys. Res., 102, 16,911-16,922.

Hsu, N. Christina, J. R. Herman, and C. J. Weaver, 2000: Determination of Radiative Forcing of Saharan Dust Using Combined TOMS and ERBE Data, J. Geophys. Res., 105, 20,649-20,661.

Hsu, N. Christina, J. R. Herman, O. Torres, B. N. Holben, D. Tanre, T. F. Eck, A. Smirnov, B. Chatenet, F. Lavenu, 1999: Comparisons of the TOMS aerosol index with Sun photometer aerosol optical thickness: Results and applications, J. Geophys. Res., 104, 6269-6279.

Joiner, J., and L. Rokke, 2000: Variational cloud-clearing with TOVS data, Q. J. R. Meteorol. Soc., 126, 725-748.

Kaufman, Y. J., D. Tanre, O. Dubovik, A. Karnieli, L. A. Remer, 2000: Absorption of sunlight by dust as inferred from satellite and ground-based remote sensing, Geophys. Res. Let., 28, 1479-1482.

Karyampudi, V. M., and T. N. Carlson, 1988: Analysis and numerical simulations of the Saharan air layer and its effect on easterly wave disturbances, J. Atmos. Sci., 45, 3102-3136.

Lin, S. J. and R. B. Rood, 1996: Multidimensional flux form semi-Lagrangian transport schemes, Mon. Wea. Rev., 124, 2046-2070.

Li, X., H. Maring, D. Savoie, K. Voss, and J. M. Prospero, 1996: Dominance of mineral dust in aerosol light-scattering in the North Atlantic trade winds, Nature, 380, 416-419.

Miller, R. L. and I. Tegen, 1998: Climate response to soil dust aerosols, J. Climate, 11, 3247-3267.

Paterson, E. M. and D. A. Gillette and B. H. Stockton, 1977: Complex index of refraction between 300 and 700 nm for Saharan Aerosols.*J. Geophys. Res.* 21, 3153-3160.

Prospero, J. M. and T. N. Carlson, 1980/81, Saharan air outbreaks over the Tropical North Atlantic, Pageoph., 119, 677-691.

Schubert, S. R., R. B. Rood and J. Pfaendtner, 1993: An assimilated dataset for earth science applications, Bull. Am. Meteorol. Soc., 74, 2331-2342.

Sokolik, N. and O. B. Toon, 1999: Incorporation of mineralogical composition into models of the radiative properties of mineral aerosol from UV to IR wavelengths, *J. Geophys. Res.* 104, 9423-9444.

Sokolik, N. and O. B. Toon, 1996: Direct radiative forcing by anthropogenic mineral aerosols, Nature, 381, 681-683.

Tegen, I. and A. A. Lacis, 1996: Modeling of particle size distribution and its influence on the radiative properties of mineral dust aerosol, J. Geophys. Res., 101, 19,237-19,244.

Tegen, I. and I. Fung, 1994: Modeling of mineral dust in the atmosphere: Sources, transport and optical thickness, J. Geophys. Res., 99, 22,897-22,914.

Twomey, S. 1977: The influence of pollution on the shortwave albedo of clouds., J. Atmos. Sci., 34, 1149-1152.

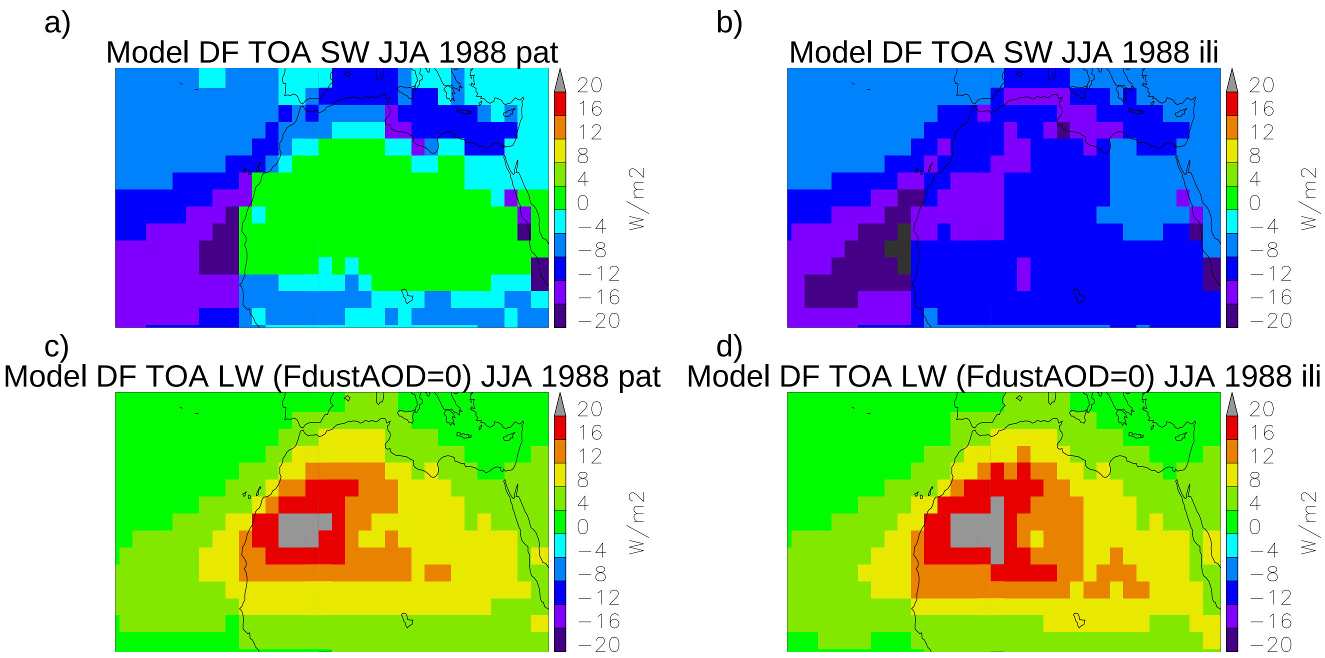

Figure 7: Average June, July and August 1988 daily TOA shortwave forcing using a) Patterson and b) Illite optical parameters. Longwave forcing $\Delta\mathbf{F}\downarrow = \mathbf{F}_{dust}\downarrow - \mathbf{F}_{dust}\downarrow$ (AOD=0) using c) Patterson and d) Illite optical parameters. Positive $\Delta\mathbf{F}\downarrow$ values describe increased incoming or decreased outgoing radiation.

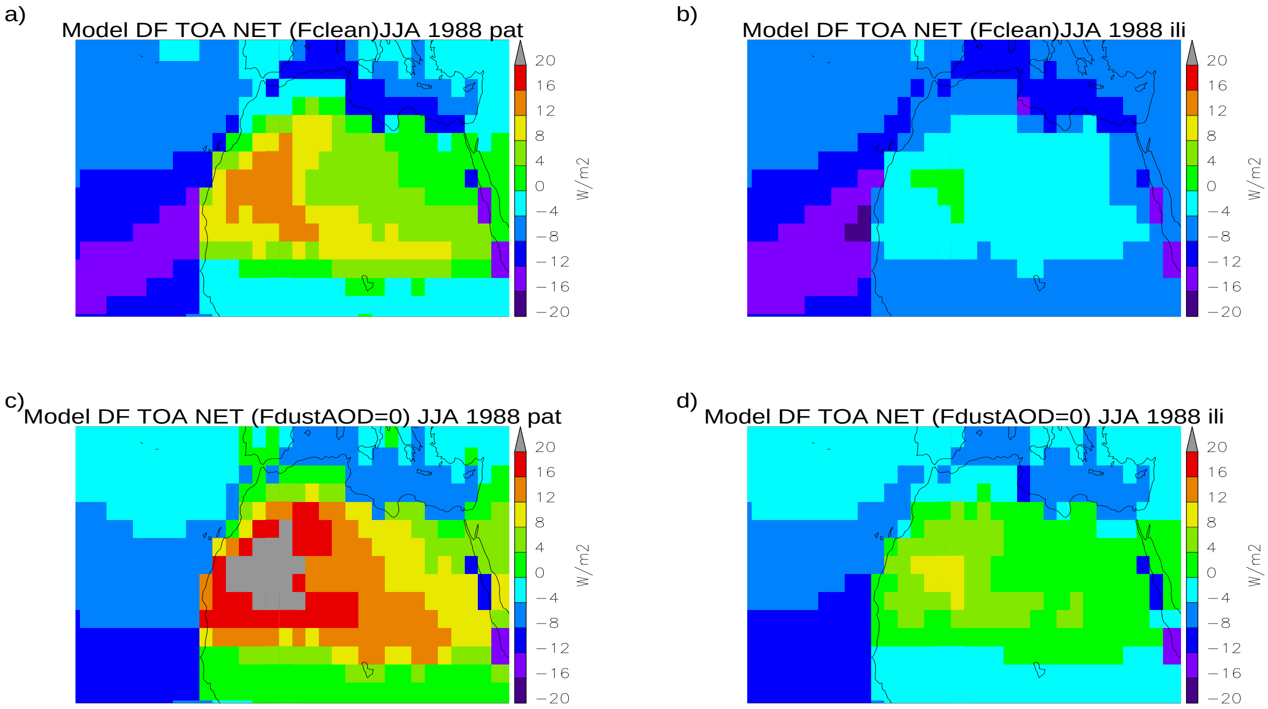

Figure 8: Average June, July and August 1988 net TOA forcing. Calculation where LW uses $\Delta\mathbf{F}\downarrow$ = $\mathbf{F}_{dust}\downarrow$ - $\mathbf{F}_{clean}\downarrow$ using a) Patterson and b) Illite optical parameters. Calculation where LW uses $\Delta\mathbf{F}\downarrow$ = $\mathbf{F}_{dust}\downarrow$ - $\mathbf{F}_{dust}\downarrow$ (AOD=0) using c) Patterson and d) Illite optical parameters. Positive $\Delta\mathbf{F}\downarrow$ values describe increased incoming or decreased outgoing radiation.

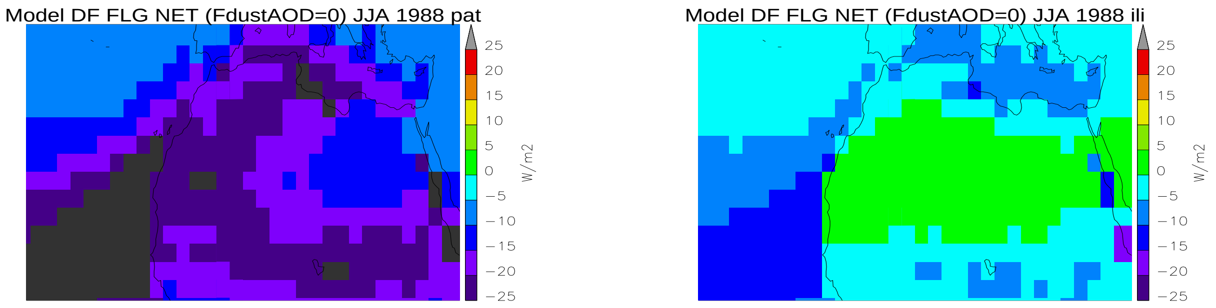

Figure 9: Average June, July and August 1988 $\Delta\mathbf{F}\downarrow$ = $\mathbf{F}_{dust}\downarrow$ - $\mathbf{F}_{dust}\downarrow$ (AOD=0) at earths surface using a) Patterson and b) Illite optical parameters. Positive $\Delta\mathbf{F}\downarrow$ values describe increased incoming or decreased outgoing radiation.

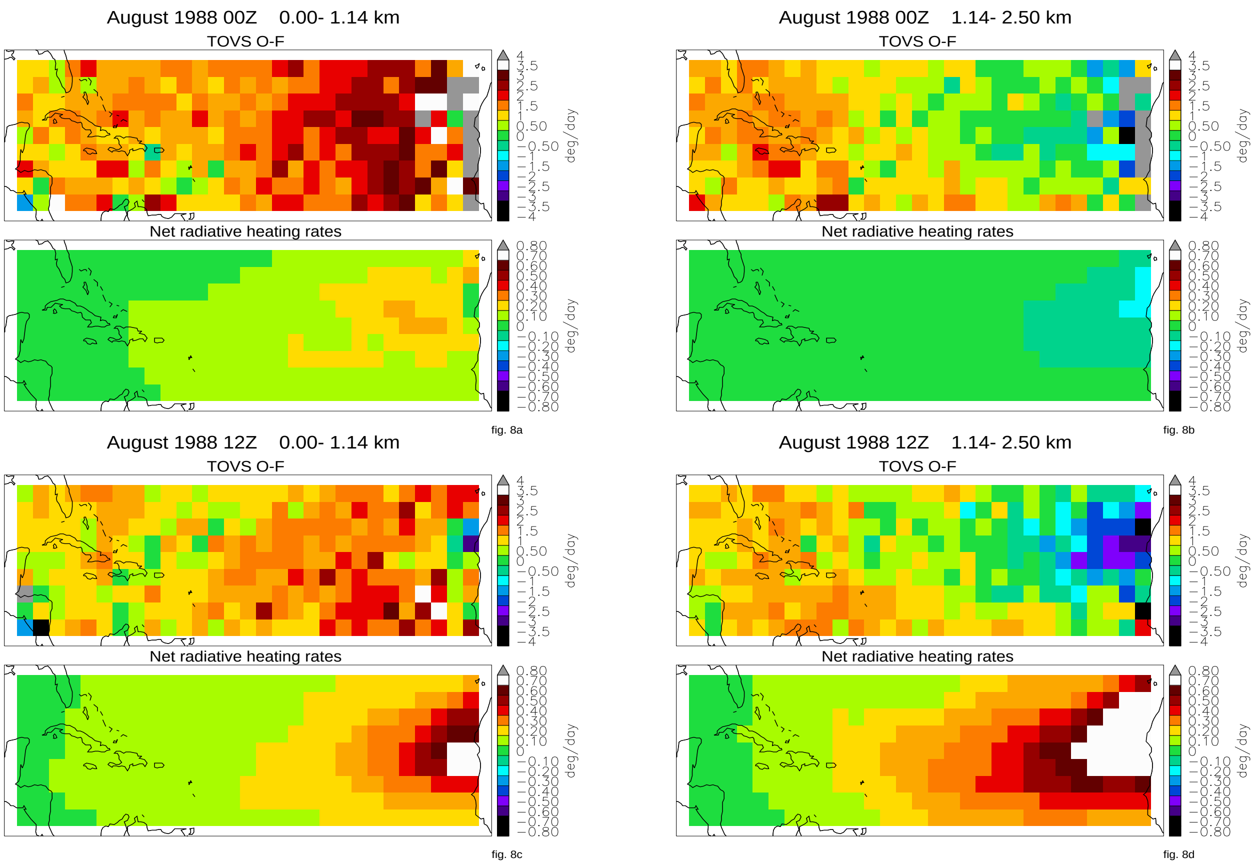

Figure 10: TOVS observed temperature minus the assimilation forecast temperature (O-F, top panel) and Net heating rates (bottom panel) calculated from simulated dust fields for a) 00Z and 0-1.14 km; b) 00Z and 1.14-2.5 km.; c) 12Z and 0-1.14 km; d) 12Z and 1.14-2.5 km. Units are in degrees (K) per day. TOVS O-F is the rate at which the temperature must be changed so that assimilation agrees with the TOVS observations.

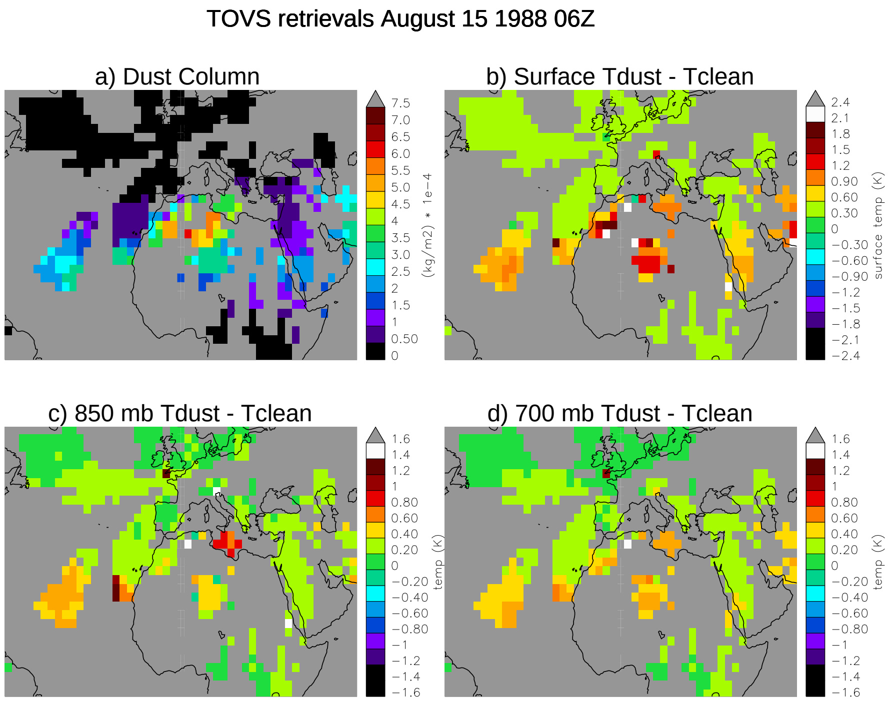

Figure 11: Differences in temperatures from two types of retrievals on 15 August 1988. One retrieval, T_{dust}, assumes dust concentrations simulated from the GOCART model. Panel a) shows the GOCART simulated aerosol column loading. The second retrieval, T_{clean} assumes no dust. Retrievals are from simulated TOVS radiances that assume the GOCART dust concentrations. Panel b) shows $T_{dust} - T_{clean}$ at earths surface, c) at 850 mb and d) at 700 mb.